pp 56–78. © Royal Aeronautical Society 2018
doi:10.1017/aer.2018.116

Sensitivity analysis of potential capacity and safety of flow corridor to self-separation parameters

B. Ye and T. Yong
bye@nuaa.edu.cn
College of Civil Aviation
Nanjing University of Aeronautics and Astronautics
Nanjing
China

National Key Laboratory of Air Traffic Flow Management
Nanjing University of Aeronautics and Astronautics
Nanjing
China

J. Shortle
Center for Air Transportation Systems Research
Department of Systems Engineering & Operations Research
George Mason University
Fairfax, VA
USA

W. Ochieng
Imperial College London
London
UK

Received 13 June 2018; revised 4 September 2018; accepted 7 September 2018.

ABSTRACT

A flow corridor is a new class of trajectory-based airspace that encloses groups of flights which fly along the same path in one direction and accept responsibility for separation from each other. A well-designed corridor could reduce the airspace complexity, decrease the workload of air traffic controllers and increase the airspace capacity. This paper analyses the impact of different self-separation parameters on capacity and conflicts of the flow corridor. Both the quantitative impact and interaction effects of pairs of parameters are evaluated using the combined discrete-continuous model and Monte Carlo simulation method. The simulation results show that although the initial separation is the dominating factor, the interactions between initial separation and separation buffer, minimum separation, extra switch buffer, extra threshold buffer and velocity difference threshold also have some significant impacts on the capacity and conflicts for the flow corridor.

Keywords: Air traffic management; Flow corridor; Self-separation; Monte Carlo simulation

NOMENCLATURE

c	tuning parameter with respect to velocity difference
C_D	drag coefficient
C_L	lift coefficient
C_{D0}	coefficient for initial climb configuration
C_{D2}	coefficient for take-off configuration
$\mathbf{C}$	tuning parameter matric with respect to velocity differences
D	drag force
D_{switch}	predicted traveling distance when switching the lane
i	the ith number of aircraft in the flow corridor
k	tuning parameter with respect to separation
$\mathbf{K}$	tuning parameter matric with respect to separations
L	lift force
m	mass of aircraft
$\mathbf{M}$	aircraft masses matrix
S	wing surface area
T	thrust
T_{ref}	thrust of the aircraft to balance the drag
v	true airspeed
$\mathrm{v}_{\mathrm{ref}}$	target velocity equal to that of the leading aircraft
$\mathbf{V_{ref}}$	target velocity matrix
W	two-lane centre distance of the corridor
x	along-track position
x_{ref}	target position along the track
$x_{\mathrm{projection}}$	projection position
$\mathbf{X}$	along-track position matrix
$\mathbf{X_{ref}}$	target position matrix
y	across-track position
z	altitude
α	angle-of-attack

https://doi.org/10.1017/aer.2018.116 Published online by Cambridge University Press

γ	flight-path angle
ζ_i	damping ratio for aircraft i
Θ	turning angle when switching the lane
ρ	air density
τ_i	time constant
ϕ	bank angle
ψ	heading angle

1.0 INTRODUCTION

A flow corridor is a new class of trajectory-based airspace that encloses groups of flights that fly along the same path in one direction and accept responsibility for separation from each other[1]. It is an airspace procedurally separated from surrounding traffic and special use airspace. The flow corridor originates from a range of similar terms such as Dynamic Airspace Super Sectors (DASS), High-Volume Tube-Shaped Sectors (HTS), Dual Airspace/Freeway, tubes and Dynamic Multi-track Airways (DMA)[2–5]. Multiple (parallel) lanes, self-separation and dynamic activation rules are the three prominent attributes of the flow corridor that are different from today's airways. A well-designed corridor should reduce airspace complexity, decrease air traffic controller workload and increase airspace capacity[6]. Since capacity, safety, cost and environmental impact are the four primary metrics used to measure the performance of an air traffic management system, in turn, influencing aircraft performance[7], the flow corridor could be shifted or adjusted to take advantage of favourable winds and optimal altitudes to reduce fuel consumption and greenhouse gas emissions. Therefore, research on capacity and safety has become an important issue for the development of flow corridors.

Previous research has addressed the initial concept design, potential benefits, network topology and optimal placement. In terms of the potential benefits, research has shown that sector loads and delays can be significantly reduced under very high traffic demands by creating very few corridors[8,9]. With regard to the required equipage and capabilities for aircraft, Automatic Dependent Surveillance-Broadcast (ADS-B) equipment, Performance Based Navigation (PBN) capability combining Area Navigation (RNAV) and Required Navigation Performance (RNP), Cockpit Display of Traffic Information (CDTI), and self-separation with lane change manoeuvres have been suggested by many researchers[10,11]. With respect to the spatial configuration and optimisation, many methods including those based on Jet routes, Delaunay triangulation, traffic density, Hough transform, user-preferred vectoring and flow-based clustering are used to identify the potential corridors[12–18]. The results from these methods have shown that the flow corridor backbones are recommended to be deployed between high-volume airports connecting congested city pairs. Until recently, limited literature has been available on aircraft operations and evaluation in the corridor. Ye et al.[19] established a discrete-event model to simulate self-separation movements of aircraft in flow corridors. Blom and Bakker[20] evaluated the safety of advanced self-separation under very high en route traffic demand. Welch[21] developed a workload-based capacity model and indicated that the capacity of one-lane tube-shaped flow corridor is more than 50% larger than that of the current nominal sector. Zhang et al.[22] used Monte-Carlo simulation with dynamic event trees to evaluate the effectiveness of subsequent safety layers that protect against collisions, and estimated that the overall safety based on the methodology is 10^{-9} collisions per flight hour. However, there is no evidence of substantive research to analyse the potential

https://doi.org/10.1017/aer.2018.116 Published online by Cambridge University Press

relationship between capacity and conflicts to aircraft self-separation parameters. Thus, it is difficult to propose comprehensive and agreed rules, guidelines or methods for the determination of the capacity under different safety levels within the corridors.

This paper addresses this gap in the research with a systematic analysis of the effect of different self-separation parameters on the capacity and conflicts of the flow corridor. The quantitative impact and interaction effects of pairs of parameters are evaluated using the combined discrete-continuous model and Monte Carlo simulation method. The results could be used to develop an optimised operational procedure for flow corridor which can safely accommodate high traffic demand with a low risk of conflicts. It should be noted that in this paper, the approach adopted is largely deterministic with safety accounted for through the anticipation of known failure modes and the incorporation of barriers. The potential effects of the unknown failure modes and uncertainty in the various relevant data, techniques and formulations are left to future research.

2.0 BASIC MODEL DESCRIPTION

2.1 Parallel-lane corridor model and basic rules

Using the existing procedures for RNAV Q-routes as a basis for flow corridor design[10,23], the flow corridor analysed here is represented by a tube of parallel high-altitude routes structure which is designed to be 80 nm long and 16 nm wide with the route centrelines 8 nm apart and located at FL350, as shown in Fig. 1. Based on the prototype spacing and passing capability for speed-independent tracks[5], pilots of the aircraft are responsible for self-separation aided by automation through Airborne Collision Avoidance System (ACAS), ADS-B and PBN capabilities including the provision of conflict resolution advisories[24]. Aircraft travel in the same direction from the entrance to exit. In the case of a faster aircraft behind a slower aircraft, pilots can adjust the velocity of the former and separation with the leading one, switch lanes for overtaking, or in extreme cases exit the corridor along paths that are at a divergence angle of 30° before the exit. Additional details of the movement rules of each aircraft in the corridor are designed as follows:

1. All aircraft initially enter the corridor with random types, velocities and separations with their leading ones, and the initial velocities are set as their target velocities in the corridor.
2. Each aircraft is in level flight along the middle line of each corridor and self-separates with the aircraft in front according to a self-separation model by adjusting its acceleration and velocity.
3. Whenever the velocity of an aircraft is higher than the average velocity of the leading one by a velocity threshold, and the separation is smaller than a specified distance threshold, it attempts to switch the lane.

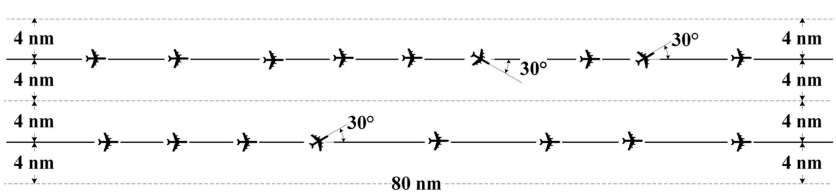

Figure 1. Structure of corridor.

https://doi.org/10.1017/aer.2018.116 Published online by Cambridge University Press

4. Whenever an aircraft gets within the minimum separation standard of the aircraft in front (loss of the minimum separation), it switches its lane or breaks out.
5. Any aircraft whose separation with its leading one is larger than a specified distance threshold value, it flies towards the target velocity.
6. The first aircraft in each lane always flies towards its target velocity.

2.2 Aircraft dynamic model

An aircraft in the flow corridor is modelled using the Point Mass Model (PMM) developed by Glover and Lygeros[25]. The aircraft motion is captured by a control system with six states (horizontal position, the altitude of the aircraft, the true airspeed, the flight path angle and the heading) and three inputs (the engine thrust, the bank angle and the angle-of-attack) as Tables 1 and 2.

The equations for level flight in the flow corridor now become

$$\begin{cases} \dot{x} = v\cos\psi\cos\gamma \\ \dot{v} = \frac{1}{m}(T\cos\alpha - D - mg\sin\gamma) \\ \dot{\psi} = \frac{1}{mv}(L + T\sin\alpha)\sin\phi \\ \dot{\gamma} = \frac{1}{mv}[(L + T\sin\alpha)\cos\phi - mg\cos\gamma] \end{cases} \quad \ldots(1)$$

where m is the mass of the aircraft and g is the gravitational acceleration. L and D denote, respectively, the lift and drag forces, which are functions of the state and the angle-of-attack as follows:

$$\begin{cases} L = \frac{C_L S\rho v^2}{2} \\ D = \frac{C_D S\rho v^2}{2} \end{cases} \quad \ldots(2)$$

Table 1
State variables

Variables	Description	Primary dimension
X	Along-track position	Along-track
v	True airspeed	Along-track
y	Across-track position	Across-track
ψ	Heading	Across-track
z	Altitude	Vertical
γ	Flight-path angle	Vertical

Table 2
Control variables

Variables	Description	Primary dimension
T	Thrust	Along-track
ϕ	Bank angle	Across-track
α	Angle-of-attack	Vertical

https://doi.org/10.1017/aer.2018.116 Published online by Cambridge University Press

where S is the surface area of the wings, ρ is the air density and C_D, C_L are aerodynamic lift and drag coefficients whose values generally depend on the phase of the fight. During the cruising phase, all commercial airliners are usually operating near trimmed flight conditions ($\gamma = \dot{\gamma} = 0$ and $\alpha \approx 0$)[26], and then the lift is represented by

$$\begin{aligned} \dot{\gamma} &= \frac{1}{m\mathrm{v}}\left[(L + T\sin\alpha)\cos\phi - mg\cos\gamma\right] = 0 \\ \Rightarrow L &= mg\frac{\cos\gamma}{\cos\phi} - T\sin\alpha = \frac{mg}{\cos\phi} \end{aligned} \quad \ldots(3)$$

Assume that the coefficient of lift C_L is set so that the lift exactly balances the weight of the aircraft. Combining the previous relationships, C_L can be calculated by

$$\begin{aligned} L &= \frac{mg}{\cos\phi} = \frac{C_L S\rho\mathrm{v}^2}{2} \\ \Rightarrow C_L &= \frac{2mg}{S\rho\mathrm{v}^2\cos\phi} \end{aligned} \quad \ldots(4)$$

The drag coefficient during the cruising phase is computed as follows:

$$C_D = C_{\mathrm{D0}} + C_{\mathrm{D2}}C_L^2 \quad \ldots(5)$$

where C_{D0} and C_{D2} are two constants.

3.0 SELF-SEPARATION PERFORMANCE IN THE FLOW CORRIDOR

3.1 Self-separation performance states definition

In order to describe self-separation performance of aircraft in the flow corridor, five discrete states are defined: Self-separation State (SS), Target Velocity Flying State (TVFS), Lane Changing State (LCS), Breakout State (BS) and Locking State (LS).

(a) Self-separation State (SS)

SS is a state in which an aircraft attempts to adjust the velocity and acceleration according to the longitudinal separation and velocity difference with its leading aircraft. An aircraft is in this state if its separation with the leading one is less than the *distance threshold* (that means, the leading aircraft is not too far in front) but larger than the *minimum separation* (the distance-based separation minima for aircraft self-separating in the flow corridor for safety operation consideration). Combining the equations of the time derivatives of the along-track positions and velocities in Equation (1), we obtain

$$\begin{cases} \dot{\mathrm{x}} = \mathrm{v}\cos\psi\cos\gamma \\ \dot{\mathrm{v}} = \frac{1}{m}(T\cos\alpha - D - mg\sin\gamma) \end{cases} \quad \ldots(6)$$

Because all the aircraft are assumed straight ($\psi = 0$ or small) and level flight ($\gamma = \dot{\gamma} = 0$, $\alpha = 0$) in the corridor, substitute the drag in Equation (2) into the above equations and get

$$\begin{cases} \dot{\mathrm{x}} \approx \mathrm{v} \\ \dot{\mathrm{v}} = \frac{T}{m} - \frac{C_D S\rho}{2m}\mathrm{v}^2 \end{cases} \quad \ldots(7)$$

https://doi.org/10.1017/aer.2018.116 Published online by Cambridge University Press

This is equivalent to a second-order equation:

$$\ddot{x} = \frac{T}{m} - \frac{C_D S \rho}{2m} \mathrm{v}^2 \quad \ldots(8)$$

Using a proportional plus derivative control for aircraft thrust (T)[26] yields

$$T = k(x_{\mathrm{ref}} - x) + c(\mathrm{v}_{\mathrm{ref}} - \mathrm{v}) + T_{\mathrm{ref}} \quad \ldots(9)$$

where T_{ref} is the thrust of the aircraft to balance the drag (Equation (2)), k and c are two tuning parameters used for keeping the target aircraft within the appropriate separation and velocity limits. x_{ref} is the target position along the track which equals to the along-track position of the leading aircraft minus the *Target Separation* (the proposed longitudinal separation to keep with the leading aircraft for safety) between the two consecutive aircraft. v_{ref} is the target velocity equal to that of the leading aircraft during the self-separating period. This leads to the second-order system as

$$\begin{aligned} \ddot{x} &= \frac{k(x_{\mathrm{ref}} - x) + c(\mathrm{v}_{\mathrm{ref}} - \mathrm{v}) + \frac{C_D S \rho}{2} \mathrm{v}^2}{m} - \frac{C_D S \rho}{2m} \mathrm{v}^2 \\ &\Rightarrow m\ddot{x} + c\dot{\mathrm{x}} + kx = kx_{\mathrm{ref}} + c\mathrm{v}_{\mathrm{ref}} \end{aligned} \quad \ldots(10)$$

Translating Equation (3) into the matrix notation, yields

$$\mathbf{X} = \begin{bmatrix} x_1 \\ \vdots \\ x_n \end{bmatrix}, \quad \mathbf{X_{ref}} = \begin{bmatrix} x_{1,\,\mathrm{ref}} \\ \vdots \\ x_{n,\,\mathrm{ref}} \end{bmatrix}, \quad \mathbf{V_{ref}} = \begin{bmatrix} v_{1,\,\mathrm{ref}} \\ \vdots \\ v_{n,\,\mathrm{ref}} \end{bmatrix}, \quad \mathbf{M} = \begin{bmatrix} m_1 & & \\ & \ddots & \\ & & m_n \end{bmatrix},$$

$$\mathbf{C} = \begin{bmatrix} c_1 & & \\ & \ddots & \\ & & c_n \end{bmatrix}, \quad \mathbf{K} = \begin{bmatrix} k_1 & & \\ & \ddots & \\ & & k_n \end{bmatrix}$$

Thus, the self-separation system in the corridor can be denoted in matrix notation is given by

$$\mathrm{M}\ddot{\mathrm{X}} + \mathrm{C}\dot{\mathrm{X}} + \mathrm{KX} = \mathrm{CV_{ref}} + \mathrm{KX_{ref}} \quad \ldots(11)$$

To calculate the value of matrix **C** and **K**, given that an un-damped natural frequency matrix is

$$\Omega = \begin{bmatrix} \omega_1 & & \\ & \ddots & \\ & & \omega_n \end{bmatrix} = \begin{bmatrix} \sqrt{\frac{k_1}{m_1}} & & \\ & \ddots & \\ & & \sqrt{\frac{k_n}{m_n}} \end{bmatrix}$$

Given also that the damping ratio of an aircraft i is

$$\zeta_i = \frac{c_i}{2\sqrt{m_i k_i}} \quad \ldots(12)$$

From the above, a time constant of τ_i can be achieved as follows, and leading to the determination of c_i

$$\tau_i = \frac{1}{\xi_i \omega_i} = \frac{2\sqrt{m_i k_i}}{c_i} \sqrt{\frac{m_i}{k_i}} = \frac{2m_i}{c_i} \Rightarrow c_i = \frac{2m_i}{\tau_i} \quad \ldots(13)$$

https://doi.org/10.1017/aer.2018.116 Published online by Cambridge University Press

A damping ratio of ζ_i can be achieved as follows, leading to the determination of k_i

$$\zeta_i = \frac{c_i}{2\sqrt{m_i k_i}} \Rightarrow k = \frac{c_i^2}{4m_i\zeta_i^2} \quad \ldots(14)$$

Using τ_1 and ζ_i as input, and with the values of **C** and **K**, the accelerations of all the aircraft for the self-separation can be calculated as Equation (5):

$$\ddot{\mathrm{X}} = \mathrm{M}^{-1}(\mathrm{K}(\mathrm{X}_{\mathrm{ref}} - \mathrm{X}) + \mathrm{C}(\mathrm{V}_{\mathrm{ref}} - \dot{\mathrm{X}})) \quad \ldots(15)$$

(b) Target Velocity Flying State (TVFS)

TVFS is a state in which an aircraft attempts to fly at its preferred target velocity without regard to the position or velocity of the aircraft in front of it. An aircraft is in this state if either (a) it is the first aircraft in the lane or (b) its leading aircraft is sufficiently far ahead (the separation is larger than the *distance threshold*) so that it does not currently need to adjust its velocity to maintain separation. Without considering the position of leading aircraft ($k = 0$), the second-order system for TVFS can be derived from Equation (10) as follows:

$$m\ddot{x} + c\dot{\mathrm{x}} + kx = k\mathrm{x}_{\mathrm{ref}} + c\mathrm{v}_{\mathrm{ref}} \Rightarrow m\ddot{x} + c\dot{\mathrm{x}} = c\mathrm{v}_{\mathrm{ref}} \quad \ldots(16)$$

where v_{ref} is the target velocity equal to its initial velocity when the aircraft enters the flow corridor. The longitudinal acceleration of the aircraft can be updated as

$$\ddot{x} = \frac{c(\mathrm{v}_{\mathrm{ref}} - \dot{\mathrm{x}})}{m} \quad \ldots(17)$$

(c) Lane Changing State (LCS)

LCS is a state in which an aircraft switches its lane to another with constant velocity for overtaking or avoiding loss of the *minimum separation*. An aircraft switches lanes under the following two situations: (a) it is traveling at a higher velocity necessitating an overtaking manoeuvre or (b) to avoid loss of the *minimum separation*. In the LCS state, the target aircraft flies a 30º (θ) path to another lane with a constant velocity as shown in Fig. 2. The constant velocity is set as the final speed before changing to the LCS state. The projection position ($x_{\mathrm{projection}}$) can be calculated based on the aircraft along-track position (x), the two-lane centre distance (W) and the turning angle (θ) as Equation (18). The traveling distance (D_{switch}) for switching the lane is shown in Equation (19), and the across track position(y) can be derived based on trigonometric function.

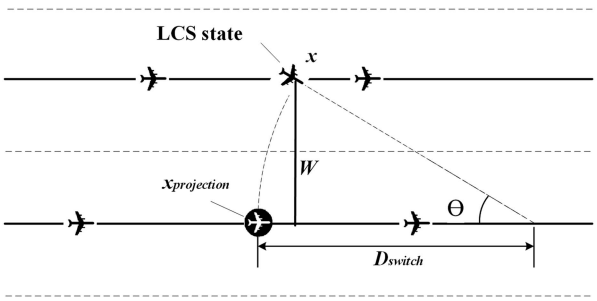

Figure 2. Lane changing state.

https://doi.org/10.1017/aer.2018.116 Published online by Cambridge University Press

$$x_{projection} = x - W \tan\frac{\theta}{2} \quad \ldots(18)$$

$$D_{switch} = \frac{W}{\sin\theta} \quad \ldots(19)$$

(d) Locking state (LS)

LS is a combined state used for safety and efficiency consideration. This state always works with the SS and TVFS states to prevent simultaneous lane changes or breakouts. When an aircraft is in the LCS, the trailing aircraft in the original corridor will be in the LS state (be locked) for one-time step in order to avoid two consecutive aircraft changing to the LCS or the BS at the same time. Furthermore, the leading and trailing aircraft in the new corridor are locked until the corridor switch procedure is finished for safety. This is to prevent two aircraft from 'crossing' in the middle while changing lanes. Figure 3 illustrates a scenario of LSs. As stated earlier, the consideration of safety is a largely deterministic process based on known failure modes and the incorporation of barriers, in this case through the LS. The effects of unknown failures and different sources of uncertainty including human factors or errors will be considered in the future to improve the models in this paper.

(e) Breakout state (BS)

An aircraft breaks out of the corridor if it cannot switch lane to avoid loss of the *minimum separation.* BS is a terminal state in which a target aircraft follows a route to breakout to the side of a corridor as shown in Fig. 4. The breakout aircraft keeps its velocity and adjusts its horizontal position until it is out of the corridor region. The trailing aircraft in the original corridor is locked for one-time step to avoid two consecutive aircraft changing to the BS or the LCS at the same time.

3.2 The main simulation algorithm

The main algorithm for self-separation is as follows: each aircraft is initialised with the SS, and the model checks the separations and velocity differences between the aircraft and their leading ones for state transition. If the current separation with the leading aircraft is larger than the *distance threshold*, the preceding aircraft transfers to the TVFS.

If the velocity difference is equal to or greater than the *velocity difference threshold*, and also the current separation is less than the *lane-switch threshold*, then the *lane-switch requirement* is

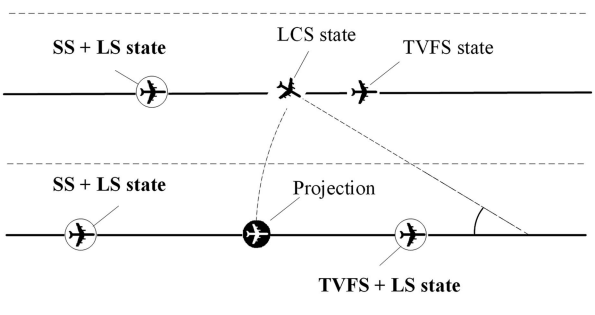

Figure 3. Locking states.

https://doi.org/10.1017/aer.2018.116 Published online by Cambridge University Press

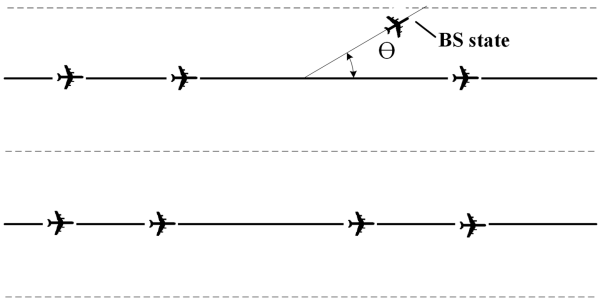

Figure 4. Breakout state.

checked. This represents a scenario where the two aircraft are close to each other and the trailing aircraft is traveling at a higher velocity necessitating an overtaking manoeuvre.

If the *lane-switch requirement* is satisfied, the trailing aircraft transfers to the LCS and flies with a constant velocity to the other lane. The aircraft in the other lane will self-separate with the lane-switching aircraft by adjusting the separation with the estimated merge point. Both the new leading and trailing aircraft in the other lane are transferred to the LS until the lane-switch manoeuvre is finished. If the lane switch requirement cannot be satisfied, the aircraft transfers to the SS state (current separation is larger than the minimum separation) or BS state (current separation is smaller than the minimum separation).

If the velocity difference is smaller than the *velocity difference threshold*, and the current separation is larger than the *minimum separation*, the trailing aircraft changes to the SS state. Otherwise, the trailing aircraft checks the *lane-switch requirement* for lane switch. This represents a case where the trailing aircraft is traveling at a velocity that is either slower or only slightly faster than the leading aircraft but the current separation cannot satisfy the minimum separation requirement, some potential conflicts might happen.

If the *lane-switch requirement* is satisfied, the trailing aircraft transfers to the LCS and some relative flights transfer to the LS; otherwise, it transfers to the BS. Figure 5 shows the main algorithm flowchart for aircraft states transitions.

The *lane-switch requirement* is defined as (a) the potential lane-switch aircraft should be in either the SS or TVFS state without being locked; (b) the potential lane-switch aircraft should make a projection of the target flight onto another lane (30° path) to find its new leading and trailing aircraft in that lane, and both of the distances between the potential lane-switch aircraft and the new leading and trailing aircraft must be larger than the *lane-switch threshold*; (c) the trailing aircraft in the new lane should also be in the SS or the TVFS without being locked.

3.3 Key parameters

3.3.1 Simulation inputs

The inputs of the simulation can be divided into four types: corridor geometry parameters, aircraft performance parameters, simulation control parameters and self-separation parameters. Among these, the self-separation parameters are the key inputs which have significant impacts on the capacity and conflicts of the corridor. Table 3 presents and describes these inputs, including the *initial separation, minimum separation, buffer separation, target separation, velocity difference threshold, distance threshold and lane-switch threshold*.

https://doi.org/10.1017/aer.2018.116 Published online by Cambridge University Press

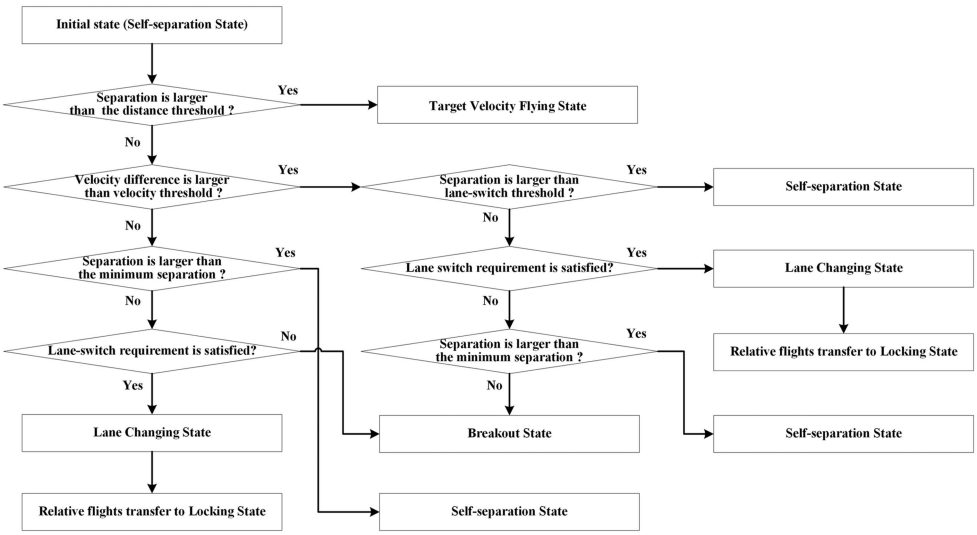

Figure 5. State transition flowchart.

Table 3
Self-separation inputs

Variables	Description
Initial separation	The initial separation between the current and the leading aircraft when the current aircraft enters the corridor
Minimum separation	The longitudinal separation minima between adjacent aircraft for safety consideration in air traffic management. It is used for trigging the lane switch or lane breakout state
Separation buffer	The extra separation that is applied to the minimum separation for safety requirement
Target separation	The target separation that each aircraft aims to keep with the leading one
Velocity difference threshold	The threshold value for the velocity difference for trigging the lane switch state
Lane-switch threshold	The threshold value for separation for trigging the lane switch state
Distance threshold	The threshold value for separation for trigging transition to the target velocity state

3.3.2 Capacity and conflict metrics

Table 4 illustrates the capacity and conflicts for the flow corridor in this paper. Capacity is measured by the flow corridor *throughput* which is defined as the number of aircraft that can fly through the flow corridor per hour (not including the breakout aircraft).

https://doi.org/10.1017/aer.2018.116 Published online by Cambridge University Press

Table 4
Capacity and safety metrics

Parameters	Description
Throughput	The inverse of the average of the corridor passing time intervals
Lane-switch rate	The proportion of aircraft that switch from one lane to another for overtaking or avoiding the loss of the minimum separation, which is considered as resolvable conflict rate
Breakout rate	The proportion of aircraft that breakout from the corridor, which is considered as un-resolvable conflict rate
Conflicts rate	The total conflict rate in the flow corridor which is obtained by the sum of lane-switch rate and breakout rate

Conflicts are measured by the *conflict rate*, *lane-switch rate* and *breakout rate* in the corridor which belongs to the strategic intent-based conflict detection and resolution safety level[22]. The *lane-switch rate* is the proportion of aircraft that switch from one lane to another for overtaking or avoiding the loss of the minimum separation which is considered as resolvable conflict rate in the corridor. The *breakout rate* is the proportion of aircraft that must leave the corridor to avoid a subsequent loss of minimum separation which is considered as un-resolvable conflict rate in the corridor. The *conflict rate* is defined as the total conflict rate for both the resolvable and un-resolvable conflict rate in the flow corridor which is obtained by the sum of *lane-switch rate* and *breakout rate*.

4.0 RESULTS ANALYSIS

4.1 Experiments design and parameters setting

The simulation program is written in the C++ language and visually verified by Google Earth. The simulated aircraft trajectories were converted to KML format, which can be read by Google Earth and displayed in an animated fashion, as in Fig. 6.

Both practical data and Pseudo-random numbers are used in the simulation. The simulation program has a total of 98 scalar parameters.

The aircraft performance parameters used in this research come from the *User Manual for the Base of Aircraft Data* (BADA)[27] published by EUROCONTROL. Eight typical aircraft types, A320, A332, A345, A380, B737, B742, B743, and B764, are selected for simulations. Table 5 shows some aircraft performance data which are taken from the BADA library, including the reference mass (m_{ref}), the maximum operational Mach number (M_{MO}), standard cruise Mach number above Mach transition altitude (M_{CR}) and maximum longitudinal acceleration for civil flights ($a_{\text{I, max}}$). Each flight enters the flow corridor with random aircraft type and follows the standard cruise Mach number, M_{CR}, the velocity and acceleration of each flight cannot be larger than the M_{MO} and $a_{\text{I, max}}$ at any time.

For the self-separation parameters' values, to make sure that the variables are independent of each other, two more parameters, which are the *extra switch-buffer* and *extra threshold-buffer*, are introduced in the experiments. Then, the *target separation* is defined as the sum of the *minimum separation* and *separation buffer*, the *lane-switch threshold* is defined as the sum of the *target separation* and *extra switch buffer*, and the *distance threshold* is defined as the sum of *lane-switch threshold* and *extra threshold buffer*. Thus, the *initial separation*,

https://doi.org/10.1017/aer.2018.116 Published online by Cambridge University Press

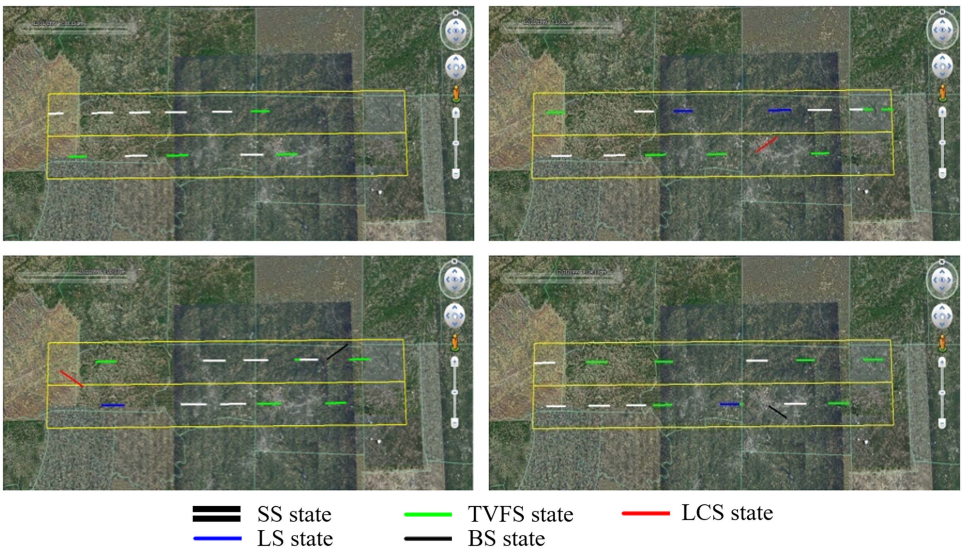

Figure 6. (Colour online) Visual verification by Google Earth.

Table 5
Aircraft performance parameters

Aircraft type	m_{ref} (tons)	M_{MO} (Mach)	M_{CR}(Mach)	$a_{I,\ max}$ (ft/s^2)
A320	64	0.82	0.78	2
A332	190	0.86	0.82	2
A345	315	0.86	0.83	2
A380	482	0.89	0.85	2
B737	60	0.82	0.78	2
B742	255.8	0.92	0.86	2
B743	310	0.9	0.85	2
B764	158.8	0.86	0.8	2

minimum separation, separation buffer, extra switch buffer, extra threshold buffer and *velocity threshold* are regarded as independent variables, and the initial values of some key simulation parameters are shown in Table 6.

4.2 Sensitivity analysis

In the experiment, in order to take into account the traffic flow pattern variations caused by different levels of severe weather, and make sure that each aircraft enters the corridor following the current ICAO aircraft separation regulations[28], the initial separation value is set as 5 nm (the longitudinal separation minima) plus a random buffer that follows an exponential distribution with the mean ranges from 1 to 10 nm. Subsequent analysis addressed the sensitivity of the other independent variables including the *separation buffer, minimum separation, extra switch-buffer, extra threshold buffer* and *velocity difference threshold.* The

https://doi.org/10.1017/aer.2018.116 Published online by Cambridge University Press

Table 6
Initial values of some key simulation parameters

Variables	Initial value	Type	Independent variables
Simulation times	10 times	Deterministic	No
Simulation time-step	6 s	Deterministic	No
Aircraft number	100,000 aircraft/lane	Deterministic	No
Time constant	12 s	Deterministic	No
Damping ration	0.707	Deterministic	No
Initial velocity	M_{CR}	Deterministic	No
Target velocity	M_{CR}	Deterministic	No
Fleet mix	Unif (0,1)	Random	No
Distance threshold	23 nm	Deterministic	No
Initial separation	5 + Exp(1) nm	Random	Yes
Separation buffer	2 nm	Deterministic	Yes
Minimum separation	5 nm	Deterministic	Yes
Extra switch buffer	2 nm	Deterministic	Yes
Extra threshold buffer	10 nm	Deterministic	Yes
Velocity difference threshold	40 Kn	Deterministic	Yes

throughput, conflict rate, breakout rate and *lane-switch rate* are four metrics used for performance evaluation.

4.2.1 Initial separation and separation buffer

Figure 7 reflects the changes in the four metrics with the increase of *separation buffer* from 0.5 nm to 10 nm in 0.5 nm steps, and other parameters are set as initial values in Table 6. In general, with the increase of *initial separation*, both the *throughputs* and *conflict rates* are reducing consistently, which are in conformity with the 'larger initial separation makes for safer flying' intuition. However, with the increase of *separation buffer*, associated curves show different change trends.

For the *throughput*, there is an obvious hump-shape configuration in the relation between the *throughput* and the *separation buffer*, but the hump shape shrinks and disappears gradually with the increase of *initial separation*. When the *initial separation* equals 5 + exp (1) nm, the *throughput* increases from 143.81 to 145.31 aircraft/hour at first, then decreases quickly to only 71.12 aircraft/hour. As the *initial separation* increases to 5 + exp (10) nm, no hump exists anymore and the *throughput* curve shows only a slight and steady decrease from 61.58 to 59.54 aircraft per hour.

For the *conflict rate*, associated curves show a similar 'decrease–increase' trend with the increase of *separation buffer*, also these 'decrease and increase' gradients are getting smaller with the increase of *separation buffer*. When the *initial separation* equals to 5 + exp (1) nm, the *conflict rate* drops drastically from 0.0248 to 0.0124 first, and then rises sharply to over 0.5223. As the *initial separation* increases to 5 + exp (10) nm, after an initial quick drop, the *conflict rate* decreases gradually to 0.0076, and then increases mildly to 0.0906. In addition, as the main components of the *conflict rate*, the *breakout rate* curves also show a similar 'decrease–increase' trend with the *conflict rate* curves while the *lane-switch rate* curves show some fluctuation variation.

These trends indicate that there is an interesting correlation between the *initial separation* and *separation buffer*. And after detailed analysis, we find the reason is that the increase of

https://doi.org/10.1017/aer.2018.116 Published online by Cambridge University Press

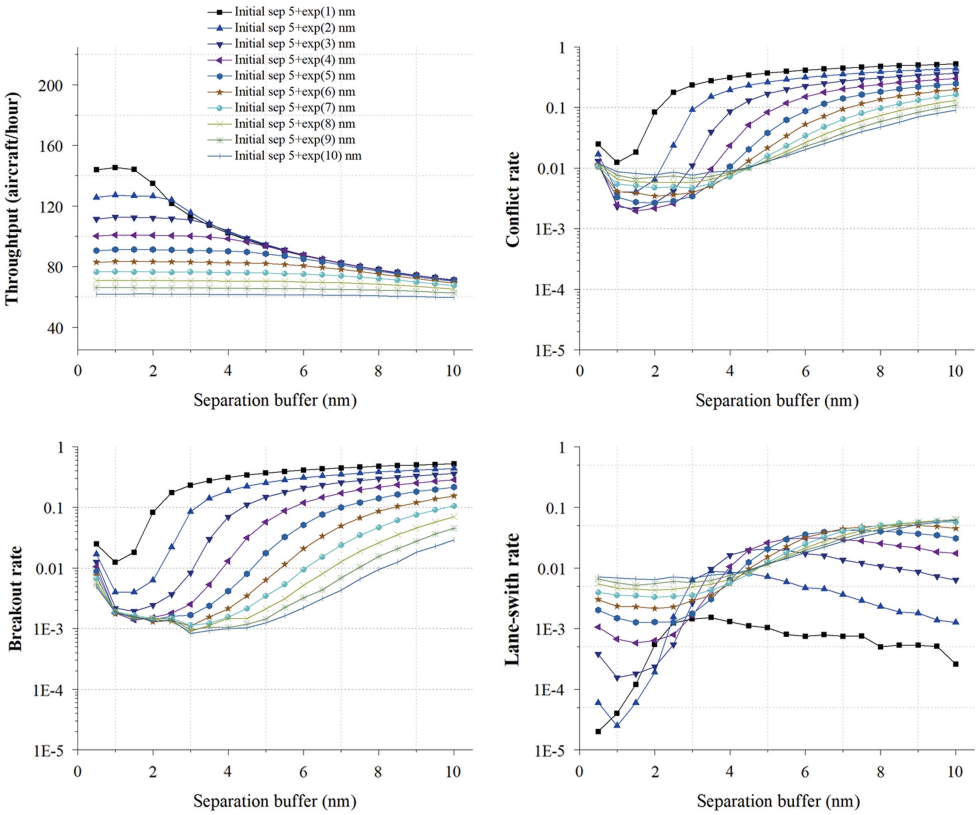

Figure 7. (Colour online) Initial separation and separation buffer.

the *separation buffer* will lead to higher *target separation*, and the extreme values of the minimum *throughput* and *conflict rate* are both obtained when the *initial separation* is close to the *target separation*. Another point worth noting is that the *lane-switch rate* not strictly followed this rule, which means that larger separation buffer also leads to larger *lane-switch threshold*, thus decreases the chance of lane-switch for the potential conflicts.

4.2.2 Initial separation and minimum separation

Figure 8 reflects the changes in the four indicators with the increase of *minimum separation* from 2 nm to 11.5 nm with 0.5 nm per step, and other parameters are set as initial values in Table 6. In general, with the increase of the *initial separation*, the *throughput* is reducing consistently while the *conflict rate* curves show an 'increase and decrease' change which breaks the intuition of 'larger initial separation makes for safer flying'. And with the increase of *separation buffer*, both the throughput and the conflict rate show a slight downward trend at the beginning, and then the throughput curves show an obvious downward trend while the conflict rate curves show a quick increase trend.

For the *throughput*, when the *initial separation* equals 5 + exp (1) nm, the throughput keeps slight decrease from 148.17 to 147.11 aircraft/hour, after that it decreases quickly to 71.18 aircraft/hour. As the *initial separation* increases to 5 + exp (10) nm, instead of the 'steady and decrease' trend, the *throughput* stays stable at about 61.54 aircraft/hour.

https://doi.org/10.1017/aer.2018.116 Published online by Cambridge University Press

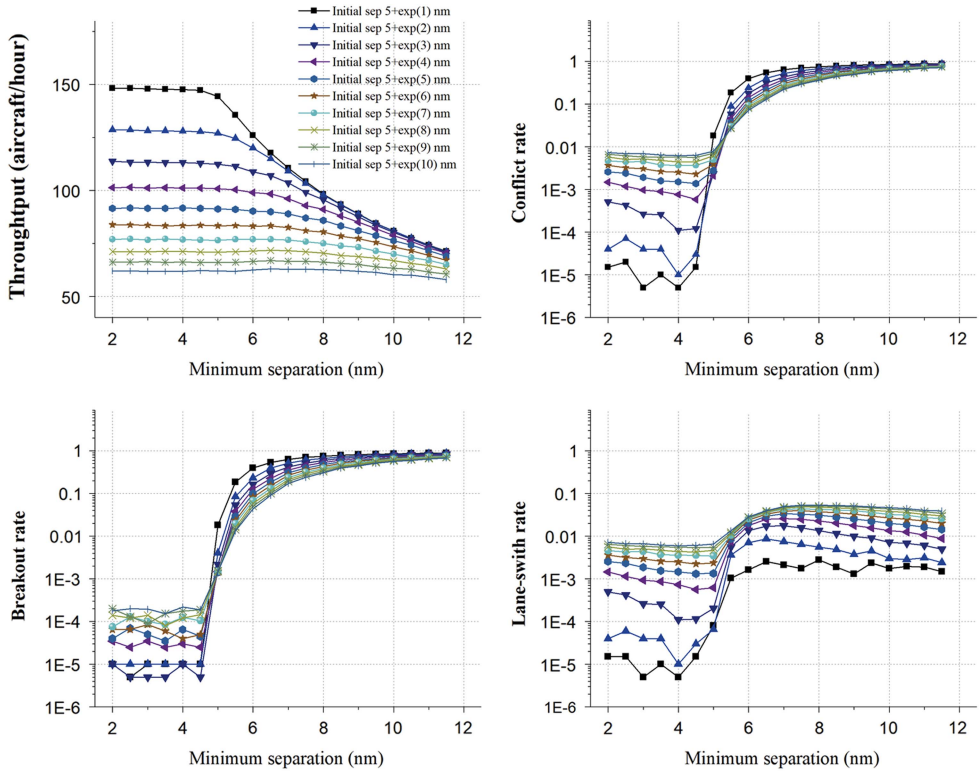

Figure 8. (Colour online) Initial separation and minimum separation.

For the *conflict rate*, when the *initial separation* equals 5 + exp (1) nm, the *conflict rate* decreases slightly from 0.000015 to 0.000005 first, and then increases to 0.8858 quickly. As the *initial separation* increases to 5 + exp (10) nm, the *conflict rate* drops slightly from 0.0073 to 0.0062 first, and then increases to 0.7187 quickly. As the principal components, both the *breakout rate* and the *lane-switch rate* show a similar 'decrease and increase' trend as the *conflict rate*. However, a noticeable trend is that the all the *lane-switch rate* curves increase monotonically with the increase of the *minimum separation* while there is some crossing point for both the *conflict rate* and *breakout rate* curves.

These trends may indicate that since the target separation will rise with the increase of the *minimum separation*, aircraft have to reduce the speeds to enlarge the separations with their leading ones, which will slow down the traffic flows and reduce the *throughputs*. Also, both the *throughput* and the *conflict rate* show tremendous changes after some threshold value in the figure which may be caused by the enlarger of the difference between the *initial separation* and the *target separation*. In addition, with the increases of the target separation, the space and chance for lane-switching are reduced gradually which leads to the decrease of the lane-switch rate again after some threshold value.

4.2.3 Initial separation and extra switch buffer

Figure 9 reflects the changes in the four indicators with the increase in the *extra switch buffer* from 0 nm to 4 nm in 0.2 nm steps, and other parameters are set as initial values in Table 6. In general, with the increase of *initial separation*, the *throughput* is consistently reducing while

https://doi.org/10.1017/aer.2018.116 Published online by Cambridge University Press

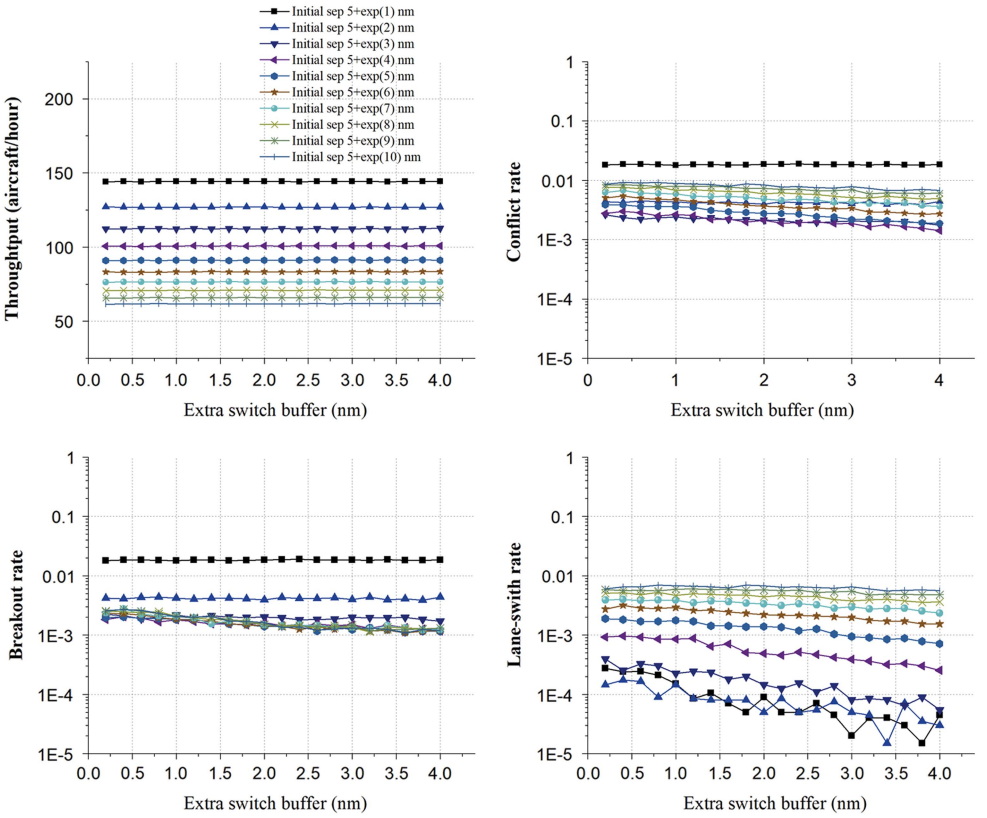

Figure 9. (Colour online) Initial separation and Extra switch-buffer.

the *conflict rate* curves show a 'decrease and increase' trend. However, with the increase of *extra switch buffer*, both the *throughput* and the *conflict rate* curves seem to fluctuate within a narrow range.

For the *throughput*, when the *initial separation* equals 5 + exp (1) nm, the *throughput* achieves the maximum mean value and stays around 144.18 aircraft/hour. As the *initial separation* increases to 5 + exp (10) nm, the *throughput* stays at around 61.79 aircraft/hour.

For the *conflict rate*, when the initial separation equals 5 + exp (1) nm, the *conflict rate* achieves the maximum mean value of 0.0184, and then decreases gradually to the minimum value at around 0.0021 as the initial separation increases to 5 + exp (3) nm. After that, the *conflict rate* rises again to 0.008 gradually with the increase of the *initial separation* to 5 + exp (10) nm. This interesting result is that the effect of the combination of the *breakout rate* and *lane-switch rate*. Both of these two metrics show a similar 'decrease and increase' change but with different extreme values. The *breakout rate* obtains the maximum mean value of 0.0183 when the *initial separation* equals 5 + exp (1) and the minimum mean value of 0.0015 when the initial separation equals 5 + exp (5). The *lane-switch rate* obtains the maximum mean value of 0.0063 when the *initial separation* equals 5 + exp (10) and the minimum mean value of 0.00008 when the initial separation equals 5 + exp (2).

https://doi.org/10.1017/aer.2018.116 Published online by Cambridge University Press

These trends may indicate that different *extra switch buffer* may has little effect on the four metrics, but with the *initial separation*, there are still some joint impacts on the conflict rates, breakout rates and lane-switch rates.

4.2.4 Initial separation and extra threshold buffer

Figure 10 reflects the changes in the four indicators with the increase in the *extra threshold buffer* from 5 nm to 14.5 nm in 0.5 nm steps, and other parameters are set as initial values in Table 6. In general, with the increase of *initial separation*, the *throughput* is consistently reducing while the *conflict rate* curves show a 'decrease and increase' trend. Also, with the increase of *extra threshold buffer*, the *throughput* seems to keep steady while the *conflict rate* curves show some downward trends.

For the *throughput*, when the *initial separation* equals 5 + exp (1) nm, the *throughput* achieves the maximum mean value of 144.18 aircraft/hour. As the *initial separation* increases to 5 + exp (10) nm, the *throughput* stays at around 61.74 aircraft/hour.

For the *conflict rate*, when the initial separation equals 5 + exp (1) nm, the *conflict rate* achieves the maximum mean value and stays around 0.0184, and when the initial separation equals 5 + exp (3) nm, the *conflict rate* achieves the minimum mean value of 0.0023. After that, the mean value of *conflict rate* rises again to 0.0086 gradually with the increase of the *initial separation* to 5 + exp (10) nm. A noticeable trend is that the *lane-switch rate* curves

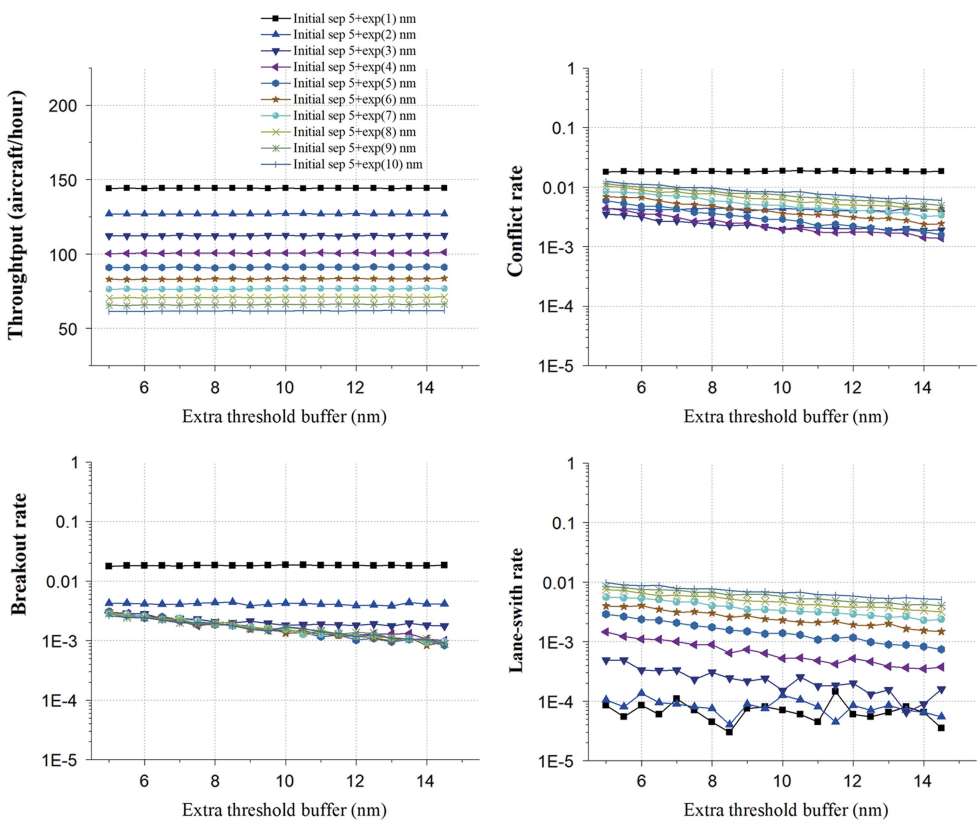

Figure 10. (Colour online) Initial separation and extra threshold buffer.

https://doi.org/10.1017/aer.2018.116 Published online by Cambridge University Press

reveal a general downward trend with the increase of the *extra threshold buffer* when the *initial separation* is larger than 5 + exp (1) nm. Also, the *breakout rate* and the *lane-switch rate* curves show the similar trends with the *lane-switch rate*, and the *breakout rate* obtains the maximum mean value of 0.0183 when the *initial separation* equals 5 + exp (1) and the minimum mean value of 0.0016 when the initial separation equals 5 + exp (5). The *lane-switch rate* obtains the maximum mean value of 0.0069 when the *initial separation* equals 5 + exp (10) and the minimum mean value of 0.00007 when the initial separation equals 5 + exp (1).

These trends may indicate that the effective range of aircraft self-separation manoeuvre will rise with the increase of distance threshold, which will reduce the probability of potential conflicts, leading to the lower breakout rates and lane-switch rates. The distance threshold has no significant effect on the throughputs, lane-switch rates and active lane-switch ratios.

4.2.5 Initial separation and velocity difference threshold

Figure 11 reflects the changes in the four indicators with the increase in the *velocity difference threshold* from 10 Kn to 110 Kn 5 Kn steps, and other parameters are set as initial values in Table 6. In general, with the increase of *initial separation*, the *throughput* is consistently

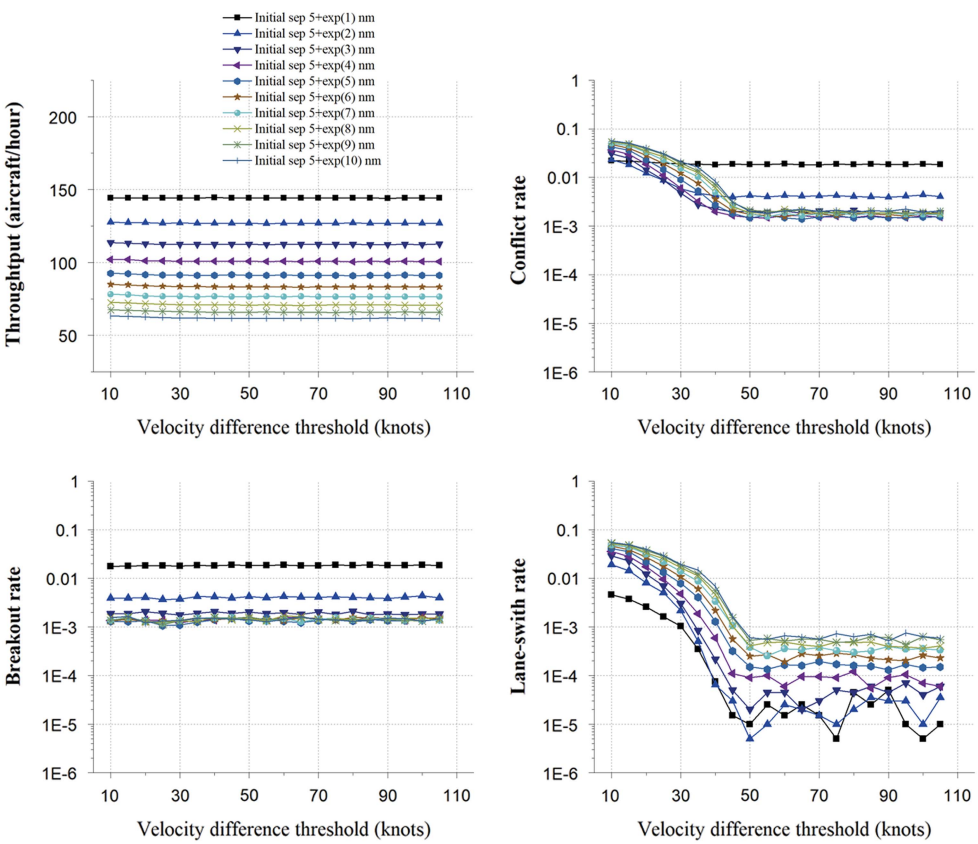

Figure 11. (Colour online) Initial separation and velocity difference threshold.

https://doi.org/10.1017/aer.2018.116 Published online by Cambridge University Press

reducing while the *conflict rate* curves show an 'increase and decrease' trend. Also, with the increase of *velocity difference threshold*, the *throughput* curves seem to keep steady while the *conflict rate* curves show a rapid decline followed by the steady trend.

For the *throughput*, when the *initial separation* equals 5 + exp (1) nm, the *throughput* achieves the maximum mean value of 144.21 aircraft/hour. As the *initial separation* increases to 5 + exp (10) nm, the *throughput* stays at around 61.92 aircraft/hour.

For the *conflict rate*, when the initial separation equals 5 + exp (1) nm, the *conflict rate* decreases to the minimum value of 0.0181 and then stays around 0.0185. When the initial separation equals 5 + exp (10) nm, the *conflict rate* decreases to the minimum value of 0.0018 and then stays around 0.0021. The curves of *breakout rate* show no obvious changes with the increase of the *velocity difference threshold*. The *breakout rate* stays around 0.0183 when the initial separation equals 5 + exp (1) nm, and decreases to around 0.0014 when the initial separation equals 5 + exp (10). However, the curves of the *lane-switch rate* show a similar trend with the *conflict rate*. When the initial separation equals 5 + exp (1) nm, the *lane-switch rate* decreases from 0.00458 to about 0.00005. When the initial separation equals 5 + exp (10) nm, it decreases from 0.0546 to about 0.0006. A noticeable trend is that all the curves begin to stabilise when the *velocity difference threshold* reaching around 50 Kn.

These trends may indicate that the trigging condition for conflicts resolution will be harder with the increase of velocity difference threshold, leading to the decreases of *breakout rates* and *lane-switch rates*. Since the maximum difference of the standard cruise Mach numbers of the eight simulation aircraft types is 0.07 Mach (about 46.3 Kn), when the velocity difference threshold is larger than 50 Kn, few aircraft can trigger the lane-switch condition, so both the *breakout rates* and *lane-switch rates* reduce from that value.

4.3 Fractional factorial analysis

The quantitative impact of each parameter and the interaction between every pairwise combination of parameters could provide a better picture of how variations in the input parameters combine to affect the capacity and safety of flow corridor. Therefore, a fractional factorial analysis is conducted to study the interactions between self-separation parameters. Based on the sensitivity analysis results, each self-separation parameter is set to either its low value or high value as given in Table 7. All combinations of these values are studied. There are $2^6 = 64$ alternative experiments conducted in total, each with 10 replications and 100,000 simulated flights. From the outputs of these experiments, the main effects (impacts of single factors) and interaction effects (impacts of pairs of factors) are estimated. Because the input values are

Table 7
Design of experiments, fractional factorial analysis

Parameter	Low	High	Unit
Initial separation (mean value)	6	12	nm
Separation buffer	1	4	nm
Minimum separation	3	5	nm
Extra switch buffer	1	4	nm
Extra threshold buffer	5	14	nm
Velocity difference threshold	20	40	knots

https://doi.org/10.1017/aer.2018.116 Published online by Cambridge University Press

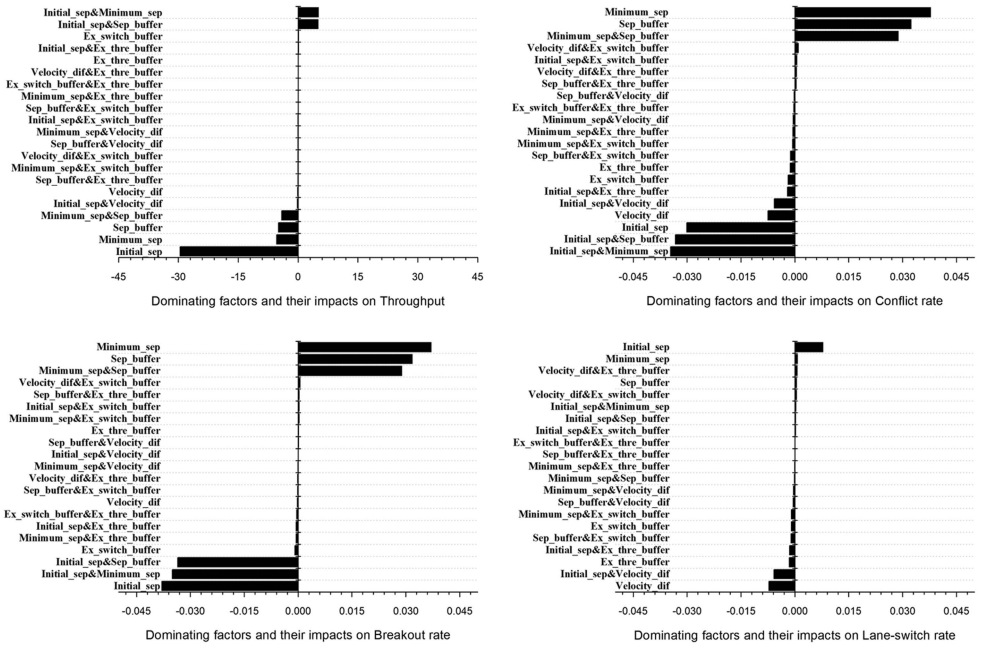

Figure 12. Full factorial ranking of effects for self-separation parameters.

'normalised' to either a low value or a high value, the resulting effects provide some measure of the relative impact of the parameters and their interactions. Of course, the results are somewhat dependent on the choice of the low and high values, and we choose the low and high value based on the sensitivity analysis above.

Figure 12 shows the main effects and interaction effects sorted by value. Both the corresponding parameter and the parameter pair are labelled on the *y*-axes. For the *throughput*, the dominating factor is initial separation which has a negative impact. It means that if the initial separation is increased, the throughput would decrease as expected. For the interaction effects of the parameter pair, the initial separation with the minimum separation and the separation buffer have similar positive impacts while the minimum separation from the separation buffer has a negative impact. For the *conflict rate*, the minimum separation, separation buffer and their interaction effects are the dominating factors which have major positive impacts, while the initial separation and its interaction effects with separation buffer and minimum separation have major negative impacts. The dominating factors of the *breakout rate* are similar to the *conflict rate* while the dominating factors of the *lane-switch rate* are the initial separation, velocity difference threshold and their interactions.

5.0 CONCLUSIONS

To study the capacity and safety for the parallel-lane flow corridor, a continuous discrete hybrid system model has been developed, which includes five aircraft states and their potential behaviours. Subsequently, this model has been used to run Monte Carlo simulations for different dense random traffic scenarios with different self-separation parameters, and a fractional factorial analysis is conducted to study the interactions between different parameters. The simulation results obtained reveal the potential characteristics of the airborne self-

https://doi.org/10.1017/aer.2018.116 Published online by Cambridge University Press

separation flow corridor concept of operations considered. The main findings in the paper are summarised below.

Although the initial separation is the dominating factor, both the separation buffer and the minimum separation have some noteworthy interaction impacts on the throughput and the conflict rate. The main reason is that the target separation, which is one of the key self-separation parameters, is composed of the separation buffer and the minimum separation. Also, a different combination of the separation buffer and the minimum separation may generate different change curves for the metrics as in Figs 6 and 7, but the extreme values seem to be obtained at the same time when the initial separation is close to the target separation. Taking these findings together, low conflict rates yield more aircraft through the flow corridor which leads to a higher throughput. From this, the main conclusion is that the interaction impacts between the separation buffer and the minimum separation are critical to the optimisation of both the capacity and safety of the self-separation flow corridor, and their interactions must be considered when designing the procedures for the self-separation flow corridor.

The results in Figs 9 and 10 show that the interactions among the initial separations, the extra switch buffer and extra threshold buffer have no obvious impacts on the flow corridor throughput, but may affect the safety metrics. All the conflicts metrics seem to decrease slightly with the increase of the extra switch buffer and extra threshold buffer. Figure 11 shows that the velocity difference threshold has a relatively low impact on the throughput, but it is an important parameter for trigging the lane switching manoeuvre. Taking all these findings together, there is a good reason to strengthen the capacity and safety evaluation for the self-separation flow corridor concept under very high traffic demands.

Because all simulations in this paper have been focused on level-flying aircraft in the parallel-lane corridor, important follow-up research is required to incorporate climbing and descending traffic in multi-layer flow corridor. Another important research direction is to conduct the sensitivity analysis for the simulation parameters such as the aircraft reaction time-lag and PD controller parameters. These require the use of the real performance and radar data for model error calibration. In addition, a third interesting direction of research is to develop a variable separation strategy based on the self-separation parameters for potential en-route congestion control if convective weather or some capacity reducing event occurs within the flow corridor.

ACKNOWLEDGEMENTS

This study was co-supported by the Natural Science Foundation of Jiangsu Province – China (No. BK20160798), China Postdoctoral Science Foundation (2018M632308) and the Fundamental Research Funds for the Central Universities – China (No. 3082015NJ20150031).

REFERENCES

1. JPDO, Concept of Operations for the Next Generation Air Transportation System (Version 3.2), 2010.
2. ALIPIO, J., CASTRO, P., KAING, H., SHAHID, N., SHERZAI, O., DONOHUE, G.L. and GRUNDMANN, K. Dynamic airspace super sectors (DASS) as high-density highways in the sky for a new US air traffic management system. Proceedings of the 2003 IEEE Systems and Information Engineering Design Symposium, 24–25 April 2003, Charlottesville, USA, pp 57-66.
3. YOUSEFI, A., DONOHUE, G.L. and SHERRY, L. High-volume tube-shape sectors (HTS): a network of high capacity ribbons connecting congested city pairs. Proceedings of the 23rd Digital Avionics Systems Conference (DASC 2004), 24–28 October 2004, Salt Lake City, USA, pp 594–593, 591.

https://doi.org/10.1017/aer.2018.116 Published online by Cambridge University Press

4. HERING, H. Air traffic freeway system for Europe. EEC-Note-No. 20/05, 2005.
5. WING, D.J., SMITH, J.C. and BALLIN, M.G. Analysis of a dynamic multi-track airway concept for air traffic management, NASA/TP-2008-215323, 2008.
6. YOUSEFI, A. and ZADEH, A.N. Dynamic allocation and benefit assessment of NextGen flow corridors, *Transportation Research Part C: Emerging Technologies*, 2013, **33**, pp 297–310.
7. ICAO, Manual on Global Performance of the Air Navigation System (First Edition), Doc 9883, 2009.
8. SRIDHAR, B., GRABBE, S., SHETH, K. and BILIMORIA, K. Initial study of tube networks for flexible airspace utilization. Proceedings of the AIAA Guidance, Navigation, and Control Conference and Exhibit, 21–24 August 2006, Keystone, USA, pp 6768.
9. GUICHARD, L., GUIBERT, S., DOHY, D. and GRAU, J. A human in the loop experiment to assess the dual airspace concept. Proceedings of the 2nd International Conference on Research in Air Transportation (ICRAT 2006), June 24–28 2006, Belgrade, Serbia and Montenegro, pp 1–11.
10. YOUSEFI, A., LARD, J. and TIMMERMAN, J. Nextgen flow corridors initial design, procedures, and display functionalities. Proceedings of the 2010 IEEE/AIAA 29th Digital Avionics Systems Conference (DASC 2010), 3–7 October 2010, Salt Lake City, USA, pp 4.D.1-1–4.D.1-19.
11. MUNDRA, A.D. and SIMONS, E.M. Self-separation corridors. Proceedings of the 2007 IEEE/AIAA 26th Digital Avionics Systems Conference (DASC 2007), 21–25 October 2007, Dallas, USA, pp 3.C.3-1–3.C.3-11.
12. XUE, M. and ZELINSKI, S. Complexity analysis of traffic in corridors-in-the-sky. Proceedings of the 10th AIAA Aviation Technology, Integration, and Operations (ATIO) Conference, 13–15 September 2010, Fort Worth, USA, pp 9112.
13. XUE, M. and KOPARDEKAR, P.H. High-capacity tube network design using the Hough transform, *J Guidance, Control, and Dynamics*, 2009, **32**, pp 788–795.
14. XUE, M. Design analysis of corridors-in-the-sky. Proceedings of the AIAA Guidance, Navigation, and Control Conference, 10–13 August 2009, Chicago, USA, pp 5859.
15. KOTECHA, P. and HWANG, I. Optimization based tube network design for the next generation air transportation system (NextGen). Proceedings of the AIAA Guidance, Navigation, and Control Conference, 10–13 August 2009, Chicago, USA, pp 5860.
16. SHETH, K.S., ISLAM, T.S. and KOPARDEKAR, P.H. Analysis of airspace tube structures. Proceedings of the IEEE/AIAA 27th Digital Avionics Systems Conference (DASC 2008), 26–30 October 2008, St. Paul, USA, pp 3.C.2-1–3.C.2-10.
17. HOFFMAN, R. and PRETE, J. Principles of airspace tube design for dynamic airspace configuration. Proceedings of the 26th Congress of ICAS and 8th AIAA ATIO, 14–19 September 2008, Alaska, USA, pp 8939.
18. GUPTA, G., SRIDHAR, B. and MUKHERJEE, A. Freeways in the sky: Exploring tube airspace design through mixed integer programming. Proceedings of the AIAA Guidance, Navigation and Control Conference and Exhibit, 18–21 August 2008, Honolulu, USA, pp 6824.
19. YE, B., HU, M. and SHORTLE, J. Collision risk-capacity tradeoff analysis of an en-route corridor model, *Chinese J Aeronautics*, 2014, **27**, pp 124–135.
20. BLOM, H.A. and BAKKER, G. Safety evaluation of advanced self-separation under very high en route traffic demand, *J Aerosp Information Systems*, 2015, **12**, pp 413–427.
21. WELCH, J. En Route Sector Capacity Model Final Report, ATC-426, 2015.
22. ZHANG, Y., SHORTLE, J. and SHERRY, L. Methodology for collision risk assessment of an airspace flow corridor concept, *Reliability Engineering & System Safety*, 2015, **142**, pp 444–455.
23. BELLE, A., SHERRY, L., YOUSEFI, A. and LARD, J. Analysis of performance of Q routes for establishing future design criteria. Proceedings of the 2010 Integrated Communications Navigation and Surveillance Conference (ICNS), 11–13 May 2010, Herndon, USA, pp B2-1–B2-7.
24. ICAO, Aircraft Operations – Volume2 Construction of Visual and Instrument Flight Procedure (Sixth Edition), Doc 8168, 2014.
25. GLOVER, W. and LYGEROS, J. A multi-aircraft model for conflict detection and resolution algorithm evaluation. IST–2001–32460, 2004.
26. PALM, W.J. *System dynamics*. McGraw-Hill Higher Education, USA; 2005.
27. EEC, User manual for the Base of Aircraft Data (BADA) Revision 3.11, EEC Technical Report 130416, 2013.
28. ICAO, Procedures for Air Navigation Services: Air Traffic Management (Sixteenth Edition), Doc 4444, 2016.

https://doi.org/10.1017/aer.2018.116 Published online by Cambridge University Press